Vol 14 No 12, December 2005
1009-1963/2005/14(12)/2565-10

Chinese Physics

© 2005 Chin. Phys. Soc.
and IOP Publishing Ltd

Nanocrystallization behaviour of a ternary amorphous alloy during isothermal annealing: a Monte Carlo simulation*

Jin Shi-Feng(金士锋)[a], Wang Wei-Min(王伟民)[a]†, Zhou Jian-Kun(周建坤)[a], Guo Hong-Xuan(国洪轩)[a], J. F. Webb[b], and Bian Xiu-Fang(边秀房)[a]

[a] *The Key Laboratory of Liquid Structure and Heredity of Materials, Shandong University, Jinan 250061, China*
[b] *School of Mechanical Engineering, Yeungnam University, 214-1 Dae-dong, Gyeongsan, Gyeongbuk 712-749, Republic of Korea*

(Received 15 March 2005; revised manuscript received 29 August 2005)

The nanocrystallization behaviour of $Zr_{70}Cu_{20}Ni_{10}$ metallic glass during isothermal annealing is studied by employing a Monte Carlo simulation incorporating with a modified Ising model and a Q-state Potts model. Based on the simulated microstructure and differential scanning calorimetry curves, we find that the low crystal-amorphous interface energy of Ni plays an important role in the nanocrystallization of primary Zr_2Ni. It is found that when $T < T_{Imax}$ (where T_{Imax} is the temperature with maximum nucleation rate), the increase of temperature results in a larger growth rate and a much finer microstructure for the primary Zr_2Ni, which accords with the microstructure evolution in "flash annealing". Finally, the Zr_2Ni/Zr_2Cu interface energy σ_G contributes to the pinning effect of the primary nano-sized Zr_2Ni grains in the later formed normal Zr_2Cu grains.

Keywords: nanocrystallization, Monte Carlo simulation, pinning effect, Ising model
PACC: 6164, 7115Q, 7460G, 0550

1. Introduction

Nanocrystalline materials can be produced in many ways, but mostly require powder compaction as a final step. An alternative approach, however, is nanocrystallization in which metallic glasses are used as precursors for creating nanocrystalline materials without any porosity.[1,2] Widely accepted conditions for achieving an ultra-fine-grained material by crystallization are small growth but large nucleation rate.[3] Properties of nanocrystalline materials depend critically on the properties of internal interfaces such as interphase boundaries and grain boundaries.[4]

Zr-based metallic glasses are mainly composed of common metals or metalloids, with high thermal stability and a wide supercooling range.[5] Through investigations in this field, it is known that the crystallization of amorphous $Zr_{70}Cu_{20}Ni_{10}$ alloy proceeds mainly by three-dimensional (3D) nucleation and diffusion-controlled growth.[6] The preferred precipitation phase during the isothermal annealing of the amorphous $Zr_{70}Cu_{20}Ni_{10}$ alloy is the fcc-Zr_2Ni phase, which exhibits a great thermal stability during annealing, and Zr_2Cu phase forms next.[7,8]

To analyse the crystallization phenomena in detail seems a hard task because of numerous and unanticipated effects. However, numerical simulation is a powerful tool to investigate the microstructural evolution during phase transitions.[9] Compared with the cell automation (CA)[10] and phase field method,[11,12] the Monte Carlo (MC) method is qualitative but simple, which permits an examination of the relationship between the configuration of atoms at the interface and the local growth conditions.[13,14] Moreover, to the authors' knowledge, there is no published microstructure simulation work on the crystallization of glasses. In this paper, we employ the MC method to simulate the nanocrystallization behaviour of the ternary metallic glass $Zr_{70}Cu_{20}Ni_{10}$. In our simulation, we ex-

*Project supported by the National Natural Science Foundation of China (Grant Nos 50301008 and 50231040) and the Shandong Young Scientists Foundation.

†Corresponding author. E-mail: weiminw@sdu.edu.cn

ploit the Ising model, a widely accepted method for studying phase transitions.[15,16] To describe the crystallization of atoms and the growth and topology of the secondary phase (Zr_2Cu) grains, the Potts model is employed—one of the most promising methods for obtaining detailed information on the topology and kinetics of microstructural evolution.[17] Anisotropy of the grain boundary, the crystal-amorphous (c/a) interface energy, and the Zr_2Ni/Zr_2Cu interface energy are considered also in our simulation model.

2. Description of the model and simulation method

2.1. The simulation model

The simulation model is based on a two-dimensional (2D) $N \times N$ square lattice with a uniform grid constant a, under periodic boundary conditions. According to the Ising model, each site of the lattice is occupied by one of the species in the amorphous state (denoted A) or in crystalline state (denoted B), with the spin state S=0, 1, 2,..., 5 for those species. If $S_i < 3$, the site i is still in an amorphous state, otherwise the site is a part of a crystallized grain. We can describe the crystallization of site i through $S_i = (S_i + 3)$. In the present system, only nearest-neighbour interactions are considered. The Ising Hamiltonian of the system then has the well-defined form[18]

$$\begin{aligned} H_{\rm I} &= -\sum_{<i,j>} E_i \\ &= -\Big[\phi_{AA}\sum_{<i,j>}(1-S_i)(1-S_j) \\ &\quad + \phi_{\rm BB}\sum_{<i,j>} S_iS_j \\ &\quad + \phi_{AB}\sum_{<i,j>}[(1-S_i)S_j + S_i(1-S_j)]\Big], \quad (1) \end{aligned}$$

where E_i represents the Ising interaction of site i with its four nearest neighbours, $< i, j >$ represents a single summation over nearest neighbours, ϕ is the interaction between the neighbouring sites, and its subscript denotes the species on the site. The spin states are S_i=0 for state A, and S_i=1 for state B. The above Hamiltonian is only for the two states A and B. In order to apply the Ising model to a phase transition in ternary alloys, we extend it as follows:

$$\begin{aligned} H_{\rm I} &= -\sum_{<i,j>} E_{\rm I} \\ &= -\sum_{<i,j>}\Big[\sum_{m,n=0}^{5}\phi_{m,n}\delta_{\rm Kr}(m,S_i)\delta_{\rm Kr}(n,S_i)\Big], \quad (2) \end{aligned}$$

where S_i and S_j represent the spin states of lattices i and j ($i,\ j\ =\ 0,\ldots,5$); $\phi_{m,n}$ ($m,\ n\ =\ 0,\ldots,5$) denotes the interaction of the nearest-neighbour spin pairs, the Ising spin states of which are m and n; and the Kronecker delta function is $\delta_{\rm Kr}(a,b)$=1, if $a = b$; $\delta_{\rm Kr}(a,b)$=0, otherwise. Through Eq.(2) we can obtain the Ising Hamiltonian of the system in a certain state. The difference between the values of the Hamiltonians for the two states is then easy to obtain.

We introduce another type of spin configuration to define the orientation of a site when we deal with a lattice of highly degenerate states. Because of the existence of internal interfaces, the interaction between domains must be considered. The highly degenerated lattice is conventionally described by the standard Potts model of spin state number $Q \geq 3$. Each lattice is then imposed on one of the Q Potts spins, i.e., $q = 0, 1 \ldots, Q-1$. A local closed area in which all sites have the same Potts spin constitutes one domain. In the most general form the nearest-neighbour interaction depends only on the relative angle between the two vectors. This is quite generally known as a system of Z (q) symmetry whose Hamiltonian reads:

$$H_{\rm P} = -\sum_{<i,j>} J(\Theta_{ij}), \quad (3)$$

$$\Theta_{ij} = 2\pi(q_i - q_j)/Q \quad q = 0, 1, \ldots, Q-1. \quad (4)$$

A grain boundary segment is defined to lie between two sites of unlike Potts spin (orientation). The energies of grain boundaries are roughly divided into the one of general high-angle boundaries and the one of small-angle boundaries, i.e. twin or high coherent boundaries, the latter is of lower energy. The ratio of the energies of the two kinds is approximately 3:1.[19] Therefore, the Potts Hamiltonian of the system can be written as:

$$\begin{aligned} H_{\rm P} &= -\sum_{<i,j>} E_{\rm P} \\ &= -\sum_{<i,j>} J[1-\delta_{\rm Kr}(q_i-q_j,0)] \\ &\quad \times \{1 - 2/3\delta_{\rm Kr}(\mathrm{int}[(q_i-q_j)/k],0)\}, \quad (5) \end{aligned}$$

where $E_{\rm P}$ stands for the Potts interaction of a site with its four nearest neighbours, J is the scale of the grain

boundary energy, q_i represents the Potts spin of site i, so $(q_i - q_j)$ here means the difference between the two spins at neighbouring sites i and j, and $\mathrm{int}[(q_i - q_j)/k]$ is the integer part of $(q_i - q_j)/k$. It is assumed that the grain boundary of relative misorientation k is the lower energy grain boundary. When $(q_i - q_j)$ equals 0, or an arbitrary positive integer between 1 and k, or that greater than k, then the values of the grain boundary energy E_{P} are zero, $J/3$, or J, respectively. So the value of E_{P} within a grain is zero. Moreover, each grain phase has its own Potts spin, so the grain boundary interaction energy between two grains of the same-phase can be obtained through Eq.(5), and the grain boundary interaction energy between different grains having different phases can be assumed to be the same as the high-angle boundary energy of a phase J.

The final Hamiltonian of the system is then given by

$$\begin{aligned} H =& H_{\mathrm{I}} + H_{\mathrm{P}} \\ =& -\sum_{<i,j>} \left\{ \left[\sum_{m,n=0}^{5} \phi_{m,n} T_{(m,S_i)} T_{(n,S_j)} \right] \right. \\ & + J[1 - \delta_{\mathrm{Kr}}(q_i - q_j, 0)] \\ & \left. \times \{1 - 2/3\delta_{\mathrm{Kr}}(\mathrm{int}[(q_i - q_j)/k], 0)\} \right\}. \end{aligned} \tag{6}$$

From Eq.(6) we can find that the Hamiltonian of the system is mainly determined by $\Phi_{m,n}$ and the boundary type. The changes that decline the system's Hamiltonian will happen with much more opportunity.

Moreover, we can easily obtain the simulated differential scanning calorimetry (DSC) curve of the crystallization process through the exothermic energy $E_{\mathrm{D}} = \Delta H = \Delta E^{\mathrm{I}} + \Delta E$. DSC is widely used in investigating the kinetic properties of phase transitions.[20]

2.2. Monte-Carlo simulation method

From Eq.(6) it can be seen that a study of the static properties is complicated and tedious. But simulation of the dynamic properties is much easier; every change of the system has been limited to the changed site (or sites) and the corresponding nearest neighbours. In the simulation we will focus on the dynamic properties of the system.

When dealing with Ising model, we use the conventional algorithm for Metropolis importance sampling:

$$P^{\mathrm{I}}_{<S_i \Rightarrow S_i+3>} = \begin{cases} \exp(-\Delta E_{\mathrm{I}}/k_{\mathrm{B}}T) & \text{if} \quad \Delta E_{\mathrm{I}} > 0; \\ 0 & \text{otherwise.} \end{cases} \tag{7}$$

where ΔE_{I} denotes the difference between the Ising interactions before and after crystallization, k_{B} is Boltzmann's constant and T the annealing temperature. The smaller the ΔE_{I} is, the bigger the $P^{\mathrm{I}}_{<Si=Si+3>}$ becomes.

The diffusion event of the system during annealing is simulated by random walk. Although vacancies play an important role in the procedure, it is verified that they do not affect the qualitative result obtained through direct spin exchange. Diffusion is simulated after a failure to crystallize using

$$p_{\mathrm{D}} = D_{\mathrm{S}} \exp(-E_{\mathrm{Q}}/k_{\mathrm{B}}T), \tag{8}$$

where D_{S} is the diffusion coefficient of species S; E_{Q} represents the average diffusion activation energy of the alloy, which is a function of the temperature. According to Janlewing and Köster[21] the diffusion activation energy of $Zr_{69.5}Cu_{12}Ni_{11}Al_{7.5}$ amorphous alloys between 600–700K is about 300kJ/mol. Because of the low diffusion coefficient of the species Ni and Zr in comparison with the species Cu, the D_{S} of species Zr, Cu and Ni in the simulation is set at 0.01:1:0.05. If the diffusion is accepted, the site concerned will exchange its Ising spin with one of its uncrystallized neighbouring sites randomly.

With the Potts model we include an important sampling developed by Xiao and co-workers,[18] which takes into account relations among all possible spin changes. The spin change $i \Leftrightarrow i'$ is associated with the following probability, which is normalized to the sum of all five probabilities (four neighbours and itself):

$$P^{\mathrm{P}}_{<i \Leftrightarrow i'>} = \frac{\exp(-\Delta E_{\mathrm{P}}/k_{\mathrm{B}}T)}{\sum\limits_{<i \Leftrightarrow i''>} \exp(-\Delta E_{\mathrm{P}}/k_{\mathrm{B}}T)}. \tag{9}$$

The most preferred spin is obviously the one with the smallest ΔE_{P}.

2.3. Simulation procedure and conditions

Simulations are performed on a 2D $N \times N = 200 \times 200$ square lattice with lattice constant a. We develop a new algorithm to scan the site of the lattice arbitrarily but evenly; each site within the system is focused on once at random in one Monte Carlo step. Doing this avoids possible distortions at the end of the simulation and makes the number of MC steps (MCS)

proportional to the annealing time. The interactions between the species of the crystal (between species of the same or different type) are obtained through bond enthalpy of the species in pure metals.[22] Because of the similarity between the liquid and amorphous alloys, interactions between species of amorphous alloys are calculated from thermal data for liquid metals with the assumption of a stable thermal capacity during the change to the amorphous phase.[23]

The energies of crystalline-amorphous (c/a) interfaces are still unavailable directly in the literature, and it is known that the measurement of solid-liquid interface energy in pure materials and alloys is difficult.[24] The measurement of the c/a interface energies seems even more difficult. Köster *et al* showed that the quasicrystalline–amorphous interface energy in Zr–Cu–Ni–Al amorphous alloys is about 13mJ/m^2 (a simulation result).[25] Meanwhile, the value for the interfaces between crystalline phases and their melts is usually more than ten times larger.[21,25] Since there is similar short-range order in the melt and amorphous state for an alloy, it is reasonable to set the average c/a interface energy $\sigma_{\rm I}^{\rm av}$ in Zr–Cu–Ni alloy at 150mJ/m^2.

The grain boundary (GB) energy, γ, is related to the value J by[19]

$$\gamma = Z'N'J, \tag{10}$$

where Z' stands for the nearest neighbour coordination number of a site, and in this paper Z'=4. N' is the number of atoms per unit area of grain boundary, the nearest neighbour distance in $Zr_{70}Cu_{20}Ni_{10}$ is about 0.29nm, so N' here is about 1.2×10^{15}/cm^2. γ is set at 490mJ/m^2, for commonly normal grain boundary energy is among 150–800mJ/m^2. The Boltzmann constant $k_{\rm B}$ is about 1.38×10^{-23}J/K. Finally, if the annealing temperature $T$is 700K, J is about $1.06k_{\rm B}T$.

Since the crystal structures of Zr_2Ni and Zr_2Cu are fcc and bct respectively, the Zr_2Ni/Zr_2Cu interface energy ($\sigma_{\rm G}$) is large and the value is also not easy to determine. We set $\sigma_{\rm G}$ at 0–4.5$k_{\rm B}T$ in the present simulation.

The procedure of the simulation is as follows:

1. Ising spins ($S < 3$) are loaded on the lattice sites according to the composition of the alloy, then the spins of the sites are set to be randomly distributed. We take this as the primary condition for amorphous alloys.

2. Site i is selected at random by a scanner, then its $E_{\rm I}$ and $E_{\rm P}$ are calculated according to the local conditions. There are two cases. In the first case, if the Ising spin of the site concerned is smaller than 3, its $P^{\rm I}$ is calculated and compared with a random number $R(0 < R < 1)$; if $R < P_{\rm I}$, the change is accepted. Otherwise, $P_{\rm D}$ is calculated using Eq.(8), another random number R' is obtained for this comparison. If $R' < P_{\rm D}$, the site will exchange its Ising spin with one of its neighbours. In the second case, if the Ising spin is 3 or larger, $P^{\rm P}$ will be calculated and the Potts spin of the site concerned will be flipped by a random number R according to Eq.(9).

3. The phase of a grain is determined by the type of its nucleus, i.e. if the first cell of a grain is the species Ni, then the grain type is fcc-Zr_2Ni, otherwise it is bct-Zr_2Cu. The Potts spins of the grains are randomly fixed during the nucleation period. After that, a new site will become the focus.

4. After each site has been scanned once, the annealing time is incremented by adding one to MCS. The procedure is repeated until a certain number of sites have crystallized.

3. Simulated results and discussion

3.1. The c/a interface energies of the species and nanocrystallization of Zr_2Ni

As mentioned above, the average c/a interface energy ($\sigma_{\rm I}^{\rm av}$) of the present system is 150mJ/m^2, the c/a interface energy for the three species ($\sigma_{\rm I}^{S}$, S=Zr, Cu, and Ni) are closely related to the intrinsic characters of these elements. To obtain a nanoscale structure the crystallization process should proceed with a large nucleation rate and slow crystal growth.[3] According to the classical theory of nucleation, the nucleation rate I can be written as[26]

$$I = I_0\exp(-16\pi\sigma^3/3RT(\Delta g)^2], \tag{11}$$

where I_0 is a constant for a given system, σ is the interface energy, R is the gas constant, T is the annealing temperature and Δg is the Gibbs energy change after crystallization.

It is quite clear from Eq.(11) that an increase in σ leads to a decline of the nucleation rate, and the low σ phase prefers to crystallize primarily with a higher nucleation rate.[4] So it can be expected that fcc- Zr_2Ni (primary phase) has the smaller c/a interface energy,[27] $\sigma_{\rm I}^{\rm Ni} < \sigma_{\rm I}^{\rm Cu}$. Because Zr has the largest atomic radius which differs greatly from the one of other species, $\sigma_{\rm I}^{\rm Zr}$ must be the largest, and we find

$\sigma_{\mathrm{I}}^{\mathrm{Ni}} < \sigma_{\mathrm{I}}^{\mathrm{Cu}} < \sigma_{\mathrm{I}}^{\mathrm{Zr}}$. We give three cases of simulation with different σ_{I}^{S} (S=Zr, Cu, and Ni) values in $Zr_{70}Cu_{20}Ni_{10}$ but a fixed $\sigma_{\mathrm{I}}^{\mathrm{av}}$ (=150mJ/m^2). The annealing temperature in our simulation is mostly 700K, and the details for the c/a interface energies of the species are shown in Table 1.

Table 1. The c/a interface energies $\sigma_{\mathrm{I}}^{\mathrm{S}}$ for different cases at 700K with a fixed average energy ($\sigma_{\mathrm{I}}^{\mathrm{av}}$=150mJ/m^2).

	$\sigma_{\mathrm{I}}^{\mathrm{Ni}}$/(mJ/m^2)	$\sigma_{\mathrm{I}}^{\mathrm{Cu}}$/(mJ/m^2)	$\sigma_{\mathrm{I}}^{\mathrm{Zr}}$/(mJ/m^2)
case 1	120	123	161
case 2	95	135	165
case 3	68	137	163

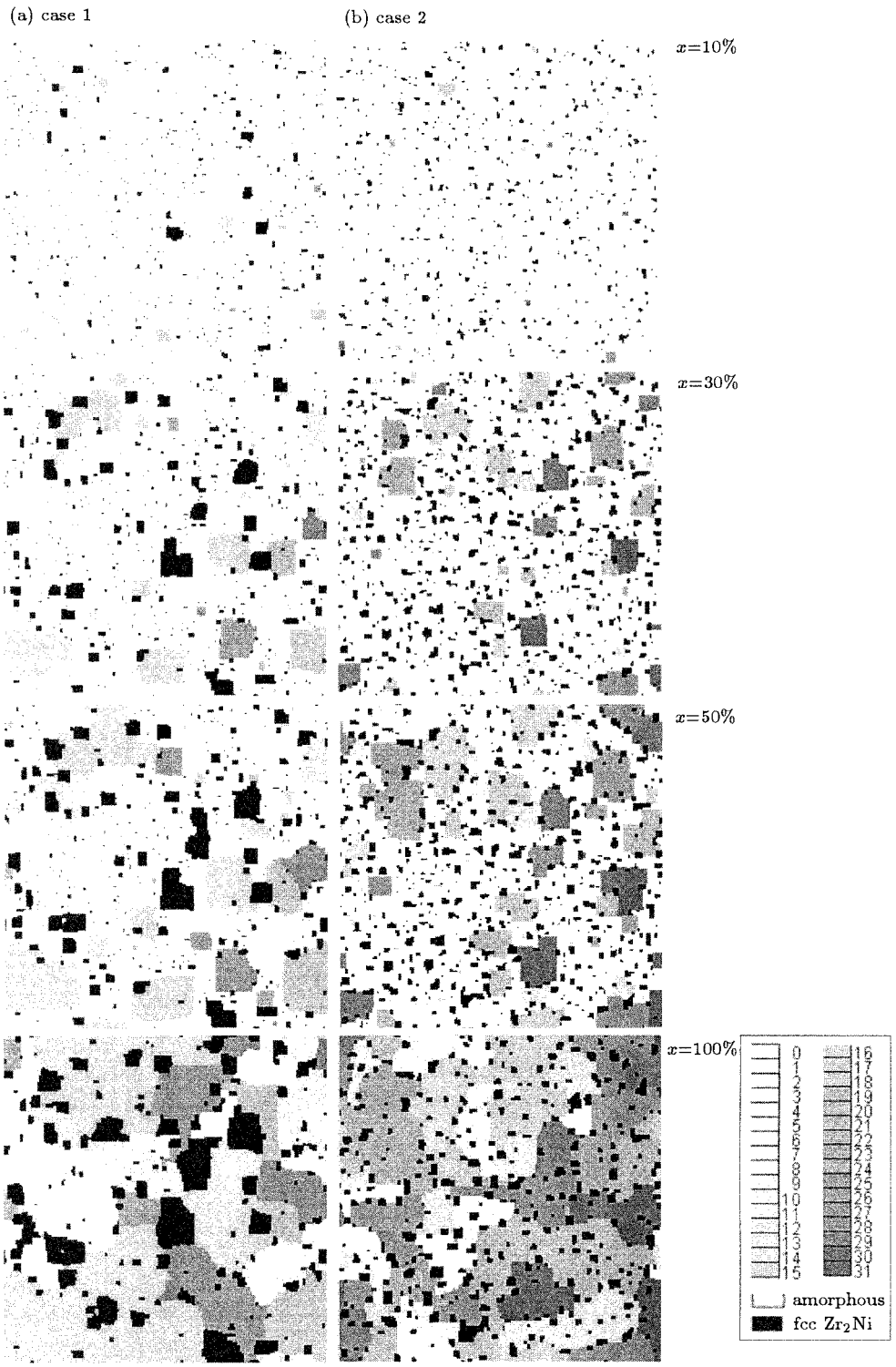


Fig.1. Temporal evolution of microstructures in the cases 1 and 2 at 700K with σ_{G}=2.0$k_{\mathrm{B}}T$. The grey scale of a lattice site in the snapshot represents the crystallographic orientation of the grain, 32 different grey scales are taken to describe the Zr_2Cu grains' orientation and the black colour is the orientation of Zr_2Ni grains.

The temporal microstructure evolution of the isothermal annealing $Zr_{70}Cu_{20}Ni_{10}$ in the cases 1 and 2 is shown in Fig.1. In the case 1, the difference between σ_I^S is small, and the crystallization behaviours of Zr_2Ni and Zr_2Cu are similar, accordingly their sizes are similar to each other as shown in Fig.1(a). In the x-ray diffraction (XRD) analysis of crystallized products of $Zr_{70}Cu_{20}Ni_{10}$, Zr_2Ni shows up as nano-sized and Zr_2Cu is normal,[7] which does not support the simulated results in Fig.1(a). In the case 2, many tiny grains appear in the primary stage of the crystallization, with few Zr_2Cu grains mixed. Finally, referring to Fig.1(b), Zr_2Cu grains become large normal grains but the Zr_2Ni grains remain to be nano-scale. This microstructure fits well the experimental results obtained from XRD and TEM analysis,[6,7] which is consistent with other alloys. For example, the ternary FeSiB alloy does not easily form a nanocrystallized phase during conventional annealing. If other elements such as Nb, Zr, Ta, etc. are added, nanocrystallites form easily, because these larger atoms are rejected from the c/a interface and decrease the interface energy.[3]

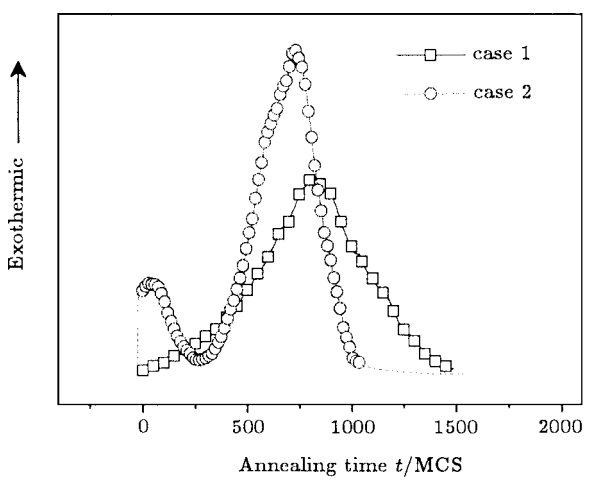


Fig.2. Variation of simulated DSC curves for the cases 2 and 3 at 700K with σ_G=2.0k_BT.

In the case 3, σ_I^{Ni} is even smaller than that in the case 2. Figure 2 gives the DSC curves in the cases 2 and 3. The curve in the case 3 exhibits two peaks; this behaviour is much different from the experimental curve in Ref.[6]. Accordingly, the case 2 is the most reasonable. Without special mentioning, all the simulations below will take the optimized σ_I^S values in the case 2, as listed in Table 1.

3.2. Kinetic properties of fcc-Zr_2Ni during nanocrystallization

Figure 3 shows the simulated nucleation rates and the average grain size of Zr_2Ni and Zr_2Cu during the isothermal annealing of $Zr_{70}Cu_{20}Ni_{10}$ at 700K. Figure 3 (a) shows clearly that Zr_2Ni has an enormous nucleation rate in the early stages of the crystallization process in comparison with the Zr_2Cu phase. According to Eq.(11), this phenomenon can be explained by the lower σ_I^{Ni} of Zr_2Ni. As the crystallization progresses, the number of easily nucleating species decreases, and the nucleation rate falls accordingly.

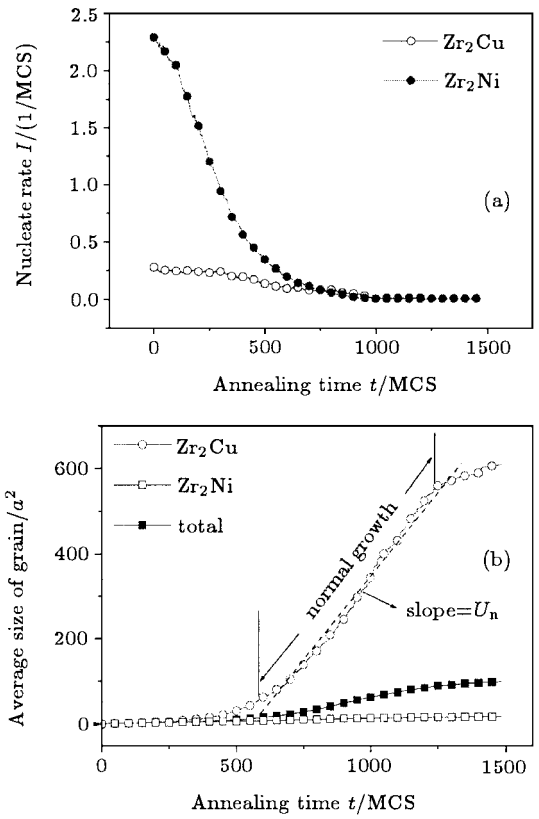


Fig.3. The nucleation rate I (a) and the average grain size A (b) of Zr_2Ni and Zr_2Cu grains versus annealing time t at 700K with σ_G=2.0k_BT.

Figure 3(b) shows the average grain size of Zr_2Cu and Zr_2Ni with annealing time, expressed as Monte Carlo Step (MCS). It is found that while the annealing process is going on, the Zr_2Cu grains grow quickly, while the Zr_2Ni grains seem stable, which reflects the fact that Zr_2Ni grains have enormous thermal stability and enjoy a much slower growth rate. After the incubation stage, the size of the Zr_2Cu grains varies as a linear function of annealing time. Hereafter, we refer to the slope of the A-t curve as the normal growth rate, denoted by U_n.

It is known that the growth is mainly divided into the interface-controlled growth and the diffusion-controlled growth. If a diffusion process is mainly determined by short-range atom jumping near the c/a interface, then according to the classical growth theory, it is the interface-controlled growth and its growth speed reads:[26,28]

$$U = a_0 v \exp\left(-\frac{\Delta G_a}{k_B T}\right)\left[1 - \exp\left(-\frac{\Delta g}{k_B T}\right)\right], \quad (12)$$

where a_0 represents the space between atoms at the surface of a new phase; ΔG_a is the activation energy for the species transferred from amorphous to crystalline phases; Δg is the driving force of the phase transition;v is the jumping frequency of atoms near the c/a interface. For Zr_2Ni, σ_I^{Ni} is low, and the Ni atoms at the c/a interface have a larger energy barrier to overcome in the crystallization (see Fig.4). This explains why the growth rate of the Zr_2Ni phase is lower than that for Zr_2Cu, as shown in Fig.3(b). Therefore, the large differences between the growth and the nucleation rates of Zr_2Ni and Zr_2Cu result in nano-scale Zr_2Ni grains and normal size grains of Zr_2Cu.

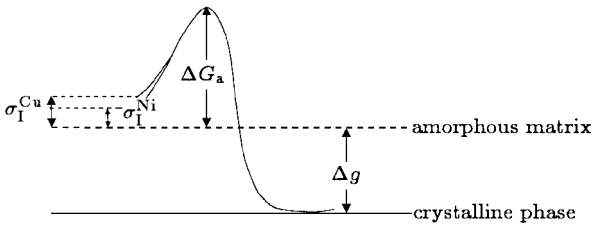


Fig.4. The energies of the phases during the crystallization of amorphous $Zr_{70}Cu_{20}Ni_{10}$.

3.3. Effect of temperature on the nanocrystallization behaviour of Zr_2Ni

Table 2 illustrates four groups of simulated parameters for the nanocrystallization behaviour under different annealing temperatures: 600, 650, 700 and 750K. It is found that the growth rate and nucleation rate of Zr_2Ni grains increase with the temperature, which can be explained by the increase of the diffusion coefficient and easier crystallization. Since both rates are increasing, the final size of the Zr_2Ni grains is determined by the ratio of the two increments. From Table 2 we know that the final nanocrystalline size is smaller when the temperature is higher, which is similar to the primary formation of the bcc Fe in FeCuSiB alloy.[3]

Table 2. Different parameters for the primary Zr_2Ni at different annealing temperatures with σ_G=2.0k_BT.

Annealing temperature/K	Maximum nucleation rate $I_{max}/(1/MCS)$	Normal growth rate $U_n/(a/MCS)$	Average final grain size $A/(a^2)$
750	0.78378	0.01596	14.0
700	0.46097	0.01140	16.0
650	0.22654	0.00809	19.5
600	0.11904	0.00585	24.0

A possible explanation of the above phenomenon is given by the growth rate - nucleation rate-temperature (U-I-T) diagram by Greer,[3,29] as shown in Fig.5. It shows that the temperature of maximum growth rate, T_{Umax} is lower than the melting temperature, T_m; and the temperature of maximum nucleation rate, T_{Imax}, is much lower than T_m. The solidification of liquid alloys usually takes place at $T > T_{Imax}$ (temperature range A) and the crystallization of metallic glasses occurs at $T_a < T_{Imax}$ (range B). According to Fig.5, an increase in annealing temperature T_a should be associated with a much greater increase of nucleation rate compared with the growth rate. So a much finer structure of very small nanocrystallites will form after high temperature annealing because of the rate difference. This phenomenon shows how to create tiny nanocrystallites, and is called high-temperature flash annealing, which now is often realized using Joule heating. For any metallic glass, the primary crystallization process can be converted into partially nanocrystallized material using this method.[3]

Figure 6 shows the size distribution of Zr_2Ni for different cases. It shows that the distribution of nanocrystalline grain sizes at high temperatures is broader than at low temperatures. According to Table 2 and Fig.5, the increase of the nucleation rate at high temperatures is much larger than the growth rate; hence a lot of tiny Zr_2Ni phases remain with $\log[A/\langle R\rangle] = -1.4$, which broaden the distribution, as shown in Fig.6(a). This suggests that the simulated structure at high temperatures is further away from equilibrium than at low temperatures after a shorter

annealing time, which can be avoided by increasing the annealing time.

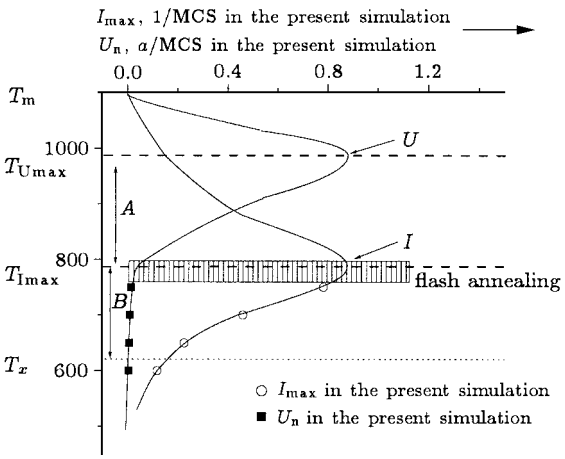


Fig.5. The simulated maximum nucleation rate I_{max} and normal growth rate U_n of primary Zr_2Ni with $\sigma_G=2.0k_BT$ and a U-I-T diagram proposed by Greer.[3,29] T_x and T_m are the crystallization temperature and the melting point of the amorphous $Zr_{70}Cu_{20}Ni_{10}$ respectively.

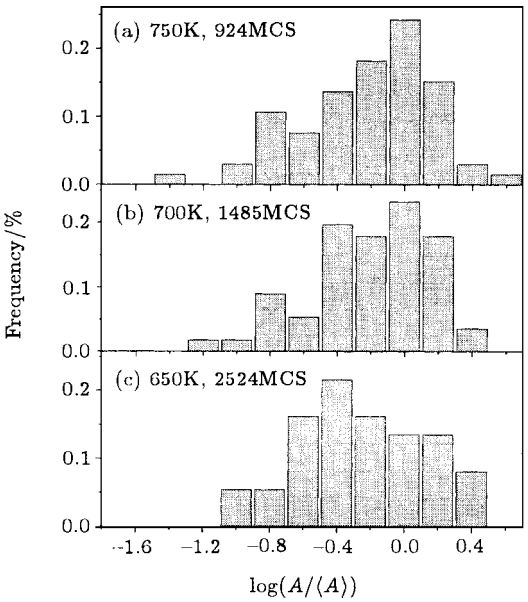


Fig.6. The size distribution of Zr_2Ni grains at different temperatures with $\sigma_G=2.0k_BT$.

3.4. Effect of primary crystalline on the growth kinetics

Figure 7 shows the simulated patterns for differ-

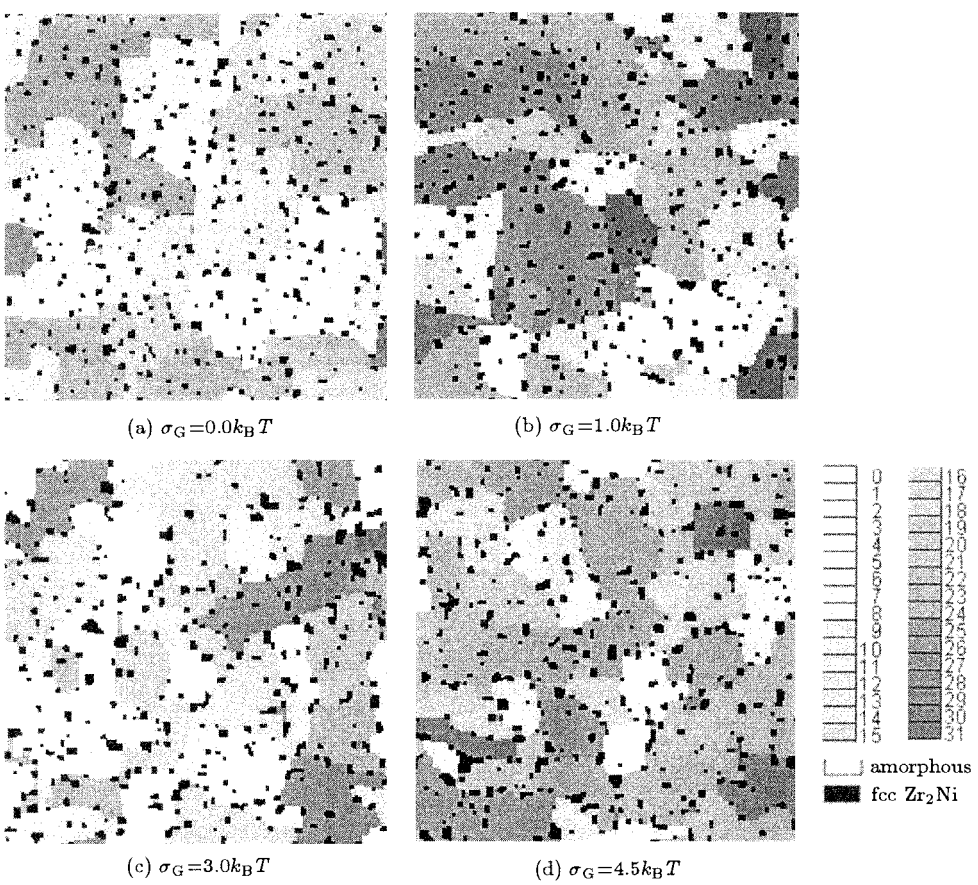


Fig.7. Patterns for various σ_G at 700K. The grey scale of a lattice site in the snapshot represents the crystallographic orientation of the Zr_2Cu grains, 32 different grey scales are taken to describe different Zr_2Cu grain orientations, and the black colour represents Zr_2Ni grains, also with different orientation.

ent values of σ_G. The Zr_2Ni phase segregates obviously on the grain boundaries when $\sigma_G > 2.0k_BT$, while they distributes uniformly in the grain and on the grain boundary when σ_G=0. The average size of the Zr_2Cu grains for σ_G=3.0 and 4.5 k_BT is obviously smaller than that when σ_G=0, suggesting that the growth is pinned largely by the primary Zr_2Ni phases.

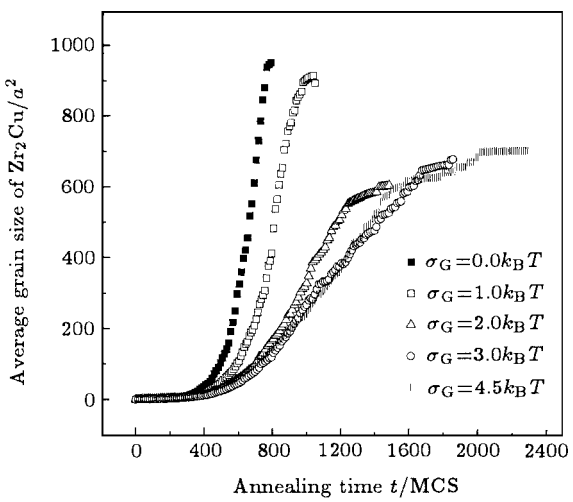


Fig.8. The size variation of Zr_2Cu grains versus annealing time for different values of σ_G at 700K.

Figure 8 presents the size of Zr_2Cu grains A against the annealing time t for different σ_G values. It is found that the normal growth rate after the incubation decreases drastically when σ_G=$2.0k_BT$. Moreover, a platform appears in the later part of the A-t curves when $\sigma_G \geq 2.0k_BT$, hence the growth of the Zr_2Cu grain is mainly divided into two stages: (1) the first stage is the slightly pinned growth of the Zr_2Cu grain; (2) the second stage is the heavily pinned growth of the Zr_2Cu grain. The decrease of the growth rate with increasing σ_G is small in the first stage, while it is large in the next stage, implying that the Zr_2Ni grains mostly have made contact with the preformed fcc-Zr_2Ni phases and their further growth is restricted. Figure 9 shows the c/a interface between a Zr_2Cu grain and an earlier formed Zr_2Ni grain. It is well known that the interface energies obey Young's equation:

$$\sigma_I^{Ni} = \sigma_I^{Cu}\cos\varphi + \sigma_G, \qquad (13)$$

where φ is the wetting angle between Zr_2Ni and Zr_2Cu grains. If σ_I^{Ni} and σ_I^{Cu} are fixed, an increase of σ_G may result in an increase of φ. From Zener's analysis, [30] the pinning force (F) of Zr_2Ni will increase according to F= -σ_I^{Cu}cosφ. Moreover, the driving force F will reach a maximum when φ reaches π.

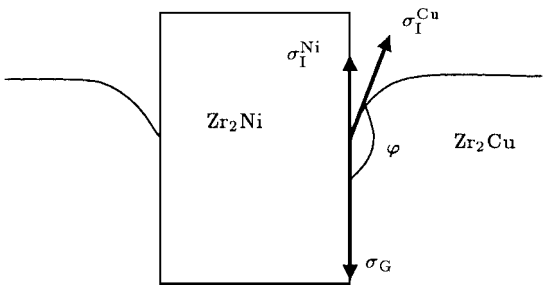


Fig.9. The c/a interface energies at the grain boundary vertex of a Zr_2Cu grain with a Zr_2Ni grain.

4. Conclusion

In summary, we have developed a Monte-Carlo approach to simulate the behaviour of nanocrystallization in ternary amorphous alloy $Zr_{70}Cu_{20}Ni_{10}$ during isothermal annealing. By investigating the simulated microstructures and DSC curves, the nanocrystallization behaviour of the primary Zr_2Ni is closely related to the low c/a interface energy σ_I^{Ni}, which results in a low growth rate U_n and a high nucleation rate I for Zr_2Ni. With increasing annealing temperature and $T < T_{Imx}$, U_n and I increase at different speeds, which agrees well with the Greer's U-I-T diagram and the microstructure evolution of "flash annealing". Finally, the pinning effect of primary Zr_2Ni on the secondary phase Zr_2Cu was found depending closely on the Zr_2Ni/Zr_2Cu interface energy σ_G.

References

[1] Köster U and Janlewing R 2003 *Materials Research Society Symposium – Proceedings* **806** 3

[2] Lu K, Wei W D and Wang J T 1992 *Script. Metall. Mater.* **24** 2319

[3] Kulik T 2001 *J. Non-Crystal. Solids* **287** 145

[4] Straumal B B, Zieba P and Gust W 2001 *Inter. J. Inorg. Mater.* **3** 1113

[5] Wang H R and Min G H 2002 *J. Mater. Sci. Lett.* **21** 1705

[6] Wang H R, Deng Y F, Gao Y L, Hui X D, Min G H, Ye Y F and Chen Y 2003 *J. Alloy Comp.* **350** 174

[7] Wang H R, Gao Y L, Min G H, Ye Y F, Chen Y, Shi Z Q and Teng X Y 2003 *J. Alloy Comp.* **349** 140

[8] Wang H R, Min G H, Gao Y L, Ye Y F and Deng Y F 2003 *J. Alloys Comp.* **354** 124

[9] Rieth M 2001 *Chin. Phys.* **10** 137

[10] Zhu M F and Hong C P 2002 *Phys. Rev.* B **66** 155428

[11] Plapp M and Karma A 2002 *Phys. Rev.* E **66** 061608

[12] Li Z J, Pan Z Y, Wei Q *et al* 2005 *Acta Phys. Sin.* **54** 2233 (in Chinese)

[13] Jackson K A, Gilmer G H and Temkin D E 1995 *Phys. Rev. Lett.* **75** 2530
[14] Beatty K M and Jackson K A 2000 *J. Crystal Growth* **211** 13
[15] Liao B, Xue Y and Chen G Z 2002 *Acta Phys. Sin.* **51** 215 (in Chinese)
[16] Shao Y Z, Zhong W R and Lin G M 2004 *Acta Phys. Sin.* **53** 3165 (in Chinese)
[17] Thorleifsson G 1995 *Nuclear Phys. B—Proc. Suppl.* **42** 731
[18] Liu J M 1998 *Phys. Rev.* B **58** 633
[19] Saito Y and Enomoto M 1992 *ISIJ Int.* **32** 267
[20] He Y 1999 *Thermo Chimica. Acta* **338** 7
[21] Janlewing R and Köster U 2001 *Mater. Sci. Eng.* A **304-306** 833
[22] Ye D L and Hu J H 2002 *Handbook on the Thermodynamic Data of Inorganic Materials* (Beijing: Press of Metallurgical industry) (in Chinese)
[23] Iida T and Guthrie R I 1993 *The Properties of Liquid Metals* (Oxford: Clarendon)
[24] Keslioğlu K, Gündüz M, Kaya H and Çadırlı E 2004 *Mater. Lett.* **58** 3067
[25] Köster U, Meindardt J, Roos S and Bush R 1997 *Mater. Sci. Eng.* A **226-228** 995
[26] Feng D 1998 *Metal Physics: Phase Transition* (Beijing: Science Press) (in Chinese)
[27] Lu K 1989 *Ph. D dissertation* (Shenyang: Institute of Metal Research) (in Chinese)
[28] Gao J, Thompson R G and Patterson B R 1997 *Acta Mater.* **45** 3653
[29] Greer A L 1996 *Metall. Mater. Trans.* **27** 549
[30] Hasegawa N *et al* 1995 *Mater. Trans. JIM* **36** 952